JACS
JOURNAL OF THE AMERICAN CHEMICAL SOCIETY

Article

pubs.acs.org/JACS

Panoramic Synthesis as an Effective Materials Discovery Tool: The System Cs/Sn/P/Se as a Test Case

Alyssa S. Haynes,[†] Constantinos C. Stoumpos,[†] Haijie Chen,[†,‡] Daniel Chica,[†] and Mercouri G. Kanatzidis*[,†,‡]

[†]Department of Chemistry, Northwestern University, Evanston, Illinois 60208, United States
[‡]Materials Science Division, Argonne National Laboratory, Lemont, Illinois 60439, United States

Supporting Information

ABSTRACT: The common approach to the synthesis of a new material involves reactions held at high temperatures under certain conditions such as heating in a robust vessel in the dark for a period until it is judged to have concluded. Analysis of the vessel contents afterward provides knowledge of the final products only. Intermediates that may form during the reaction process remain unknown. This lack of awareness of transient intermediates represents lost opportunities for discovering materials or understanding how the final products form. Here we present new results using an emerging in situ monitoring approach that shows high potential in discovering new compounds. In situ synchrotron X-ray diffraction studies were conducted in the Cs/Sn/P/Se system. Powder mixtures of Cs_2Se_2, Sn, and PSe_2 were heated to 650 °C and then cooled to room temperature while acquiring consecutive in situ synchrotron diffraction patterns from the beginning to the end of the reaction process. The diffraction data was translated into the relationship of phases present versus temperature. Seven known crystalline phases were observed to form on warming in the experiment: Sn, Cs_2Se_3, Cs_4Se_{16}, Cs_2Se_5, $Cs_2Sn_2Se_6$, $Cs_4P_2Se_9$, and $Cs_2P_2Se_8$. Six unknown phases were also detected; using the in situ synchrotron data as a guide three of them were isolated and characterized ex situ. These are $Cs_4Sn(P_2Se_6)_2$, α-$Cs_2SnP_2Se_6$, and $Cs_4(Sn_3Se_8)[Sn(P_2Se_6)]_2$. $Cs_4(Sn_3Se_8)[Sn(P_2Se_6)]_2$ is a two-dimensional compound that behaves as an n-type doped semiconductor below 50 K and acts more like a semimetal at higher temperatures. Because all crystalline phases are revealed during the reaction, we call this approach "panoramic synthesis".

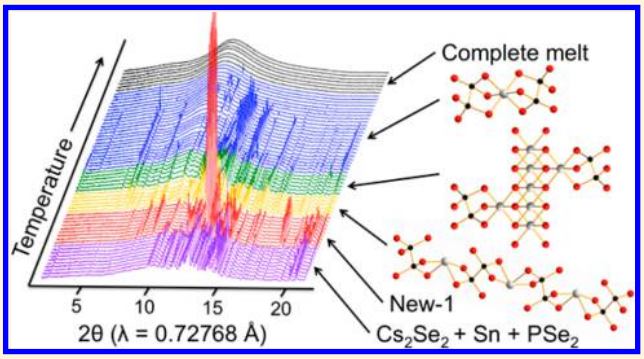

INTRODUCTION

Solid state synthesis methods for materials discovery such as the molten salt flux and solvothermal techniques have been developed to overcome problems of low diffusion and energy-minimum thermodynamic products observed with traditional "heat and beat" synthesis.[1−9] However, with current solid state synthetic techniques, we can only observe the final products. We generally do not know if these products form on heating, soaking, or cooling or how long they survive in the reaction. In this regard, our syntheses are "blind" as we are unaware of any interesting intermediates and mechanistic insight they would provide.

As a way to overcome these barriers, we have proposed a materials discovery method, which allows us to examine the entire synthetic reaction process using in situ synchrotron powder X-ray diffraction (PXRD).[10] By using temperature as a variable, the relationships among phases can be probed as the reaction proceeds. The goal is to utilize in situ synchrotron PXRD to uncover and characterize phases not accessible through traditional "blind" synthesis.

In situ synchrotron X-ray diffraction (XRD) studies have previously been employed to monitor the formation and growth of crystalline inorganic solids, and most studies have used hydrothermal,[11−15] solvothermal,[16−18] sol−gel,[14,19,20] molten salt flux,[10,21] ion-thermal,[22,23] or surfactant-thermal methods.[23,24] The majority of these investigations aimed to understand the reaction mechanism, and some studies compared syntheses using different parameters (e.g., temperature, pH, source materials, stoichiometry) to determine how the reaction pathway was affected. Many of these experiments revealed previously unknown intermediates; however, only melt-quench reactions were employed to isolate the intermediates ex situ, and none were successful.[11,13−16,20] The one exception is our previous in situ synchrotron PXRD study with the goal of discovering metastable inorganic materials.[10] We showed that even well-investigated systems of K/Cu/S and K/Sn/S still had new materials to yield that were recovered ex situ. Through these experiments, four known and four new phases were observed whose structures were solved and refined using the in situ PXRD as a guide.

Received: May 25, 2017
Published: June 30, 2017

DOI: 10.1021/jacs.7b05423
J. Am. Chem. Soc. 2017, 139, 10814−10821

Additionally, we have conducted in situ synchrotron PXRD measurements on amorphous $CsPSe_6$, which uncovered the crystallization of the new phase, β-$CsPSe_6$, and its phase transition to the known α-$CsPSe_6$.[25] The energy of the phase transition had been too low to be detected via differential thermal analysis (DTA) so the in situ experiment was needed to accurately observe the kinetics of the system. Using the information obtained from these experiments, we successfully isolated and characterized β-$CsPSe_6$ ex situ and discovered it possessed unique perpendicular chain packing within the structure. Therefore, these early examples point to the high utility of in situ synchrotron XRD studies as a direct means to understand the details of a synthetic reaction. This approach allows us to become aware not only of the final products but of all the crystalline intermediates as well as when they form, how long they exist, etc. This information is crucial to design a successful synthesis for them as we have done in this paper.

Herein we have applied this in situ PXRD approach to the Cs/Sn/P/Se system as a new model to further explore its power to help discover new phases. We chose this system because we have extensive expertise in the synthesis and study of chalcophosphate compounds.[26] Chalcophosphates have useful properties including reversible phase transitions,[27−31] ferroelectricity,[32] photoluminescence,[33,34] γ-ray detection,[35] and nonlinear optics.[25,36−39] Powder mixtures of Cs_2Se_2, Sn, and PSe_2 were heated to 650 °C then cooled while continuously monitoring the crystalline phases present with in situ synchrotron PXRD. From this data, we created a phase versus temperature map containing seven known compounds (Sn,[40] Cs_2Se_3,[41] Cs_4Se_{16},[42] Cs_2Se_5,[43] $Cs_2Sn_2Se_6$,[44] $Cs_4P_2Se_9$,[45] and $Cs_2P_2Se_8$[36]) and six unknowns. Our experiments reveal that the phase space is very rich on heating, but only one unknown crystalline phase ultimately forms on cooling.

Using the in situ synchrotron PXRD data as a guide, we successfully synthesized and determined the structures of three new tin selenophosphates. The first one, $Cs_4Sn(P_2Se_6)_2$, contains molecular ions of $[Sn(P_2Se_6)_2]^{4-}$, with octahedrally coordinated Sn^{4+} sandwiched between two $[P_2Se_6]^{4-}$ units. The second, α-$Cs_2SnP_2Se_6$, features $^1/_\infty[SnP_2Se_6]^{2-}$ chains with Sn^{2+} ions adopting a seesaw coordination geometry. The third compound was $Cs_4(Sn_3Se_8)[Sn(P_2Se_6)]_2$, a complex phase comprising of defective $SnSe_2$ layers, formulated as $^2/_\infty[Sn_3Se_8]^{4-}$, decorated on both sides of the layers with terminal $[Sn(P_2Se_6)]$ groups. These groups bind to the $^2/_\infty[Sn_3Se_8]^{4-}$ layers through three selenium ions that complete the octahedral coordination of the Sn^{4+} ions. $Cs_4(Sn_3Se_8)[Sn(P_2Se_6)]_2$ displays semimetallic behavior above 50 K and n-type doped semiconductor properties at lower temperatures.

EXPERIMENTAL SECTION

Reagents. All chemicals were used as obtained: cesium metal (99.9+%, Strem Chemicals, Inc., Newburyport, MA); tin powder (99.5% Sigma-Aldrich, St. Louis, MO); red phosphorus powder (99%, Sigma-Aldrich, St. Louis, MO); selenium pellets (99.99%, Sigma-Aldrich, St. Louis, MO). Cs_2Se and Cs_2Se_2 were synthesized by reacting stoichiometric amounts of the elements in liquid ammonia as described elsewhere.[46,47] Glassy PSe_2 was formed by reacting P (0.082 g, 2.65 mmol) and Se (0.418 g, 5.29 mmol) under an evacuation of $\sim10^{-4}$ mbar at 600 °C for 12 h. P_2Se_5 was made by reacting a stoichiometric ratio of elements using traditional solid state synthesis as described previously.[47]

Preparation of Starting Material for In Situ Synchrotron PXRD. Amounts listed below of Cs_2Se_2, Sn, and PSe_2 were combined in a mortar in a dry, N_2 atmosphere glovebox. The reactants in a mortar were ground with a pestle and mixed with a spatula for ~10 min after the mixture looked homogeneous. The powder mixture was loaded into 0.3 mm outer diameter fused silica capillaries and packed tightly to ~1 cm in length of the capillary. A layer of fused silica granules (63−90 μm) were added and served as the point of sealing of the capillary while keeping the tight packing of the powder. The capillaries were flame-sealed under an evacuation of $\sim10^{-4}$ mbar.

Sn1: Cs_2Se_2 (0.085 g, 0.20 mmol), Sn (0.012 g, 0.10 mmol), PSe_2 (0.076 g, 0.40 mmol).

Sn2: Cs_2Se_2 (0.085 g, 0.20 mmol), Sn (0.024 g, 0.20 mmol), PSe_2 (0.076 g, 0.40 mmol).

Sn3: Cs_2Se_2 (0.085 g, 0.20 mmol), Sn (0.047 g, 0.40 mmol), PSe_2 (0.076 g, 0.40 mmol).

Ex Situ Synthesis of $Cs_4Sn(P_2Se_6)_2$ (New-6). Amounts of Cs_2Se (0.169 g, 0.40 mmol), Sn (0.024 g, 0.20 mmol), P (0.025 g, 0.80 mmol), and Se (0.126 g, 1.6 mmol) were combined in a 9 mm carbon-coated fused silica tube in a dry, nitrogen-filled environment then flame-sealed after evacuating the tube to $\sim10^{-4}$ mbar. The tube was placed in a furnace and heated to 650 °C, soaked for 10 h, then cooled to 250 °C in 10 h where the furnace was turned off to allow the tube to cool to room temperature. The product contained black hexagonal plate crystals of $Cs_4Sn(P_2Se_6)_2$ (100%), which are air and water stable. Energy dispersive X-ray spectroscopy (EDS) gave an average composition of multiple crystals of $Cs_{3.8}SnP_{4.2}Se_{11.7}$.

Ex Situ Synthesis of α-$Cs_2SnP_2Se_6$ (New-4). Cs_2Se (0.169 g, 0.40 mmol), Sn (0.048 g, 0.40 mmol), P (0.050 g, 1.6 mmol), and Se (0.568 g, 7.2 mmol) were combined in a carbon-coated fused silica 9 mm tube in a dry, N_2 atmosphere glovebox. The tube was evacuated to $\sim10^{-4}$ mbar, flame-sealed, then subjected to a heating profile of heating to 650 °C, soaking for 10 h, then cooling to room temperature in 15 h. The product contained translucent orange rod crystals of α-$Cs_2SnP_2Se_6$ (85%) and SnSe (15%).[48] EDS gave an average composition of multiple crystals of $Cs_{1.9}SnP_{2.2}Se_{5.5}$. α-$Cs_2SnP_2Se_6$ was stored in an evacuated desiccator because it is air and water sensitive.

Ex Situ Synthesis of $Cs_4(Sn_3Se_8)[Sn(P_2Se_6)]_2$ (New-5). A mixture of Cs_2Se (0.276 g, 0.80 mmol), Sn (0.237 g, 2.0 mmol), P (0.050 g, 1.6 mmol), and Se (0.568 g, 7.2 mmol) were loaded into a 9 mm carbon-coated fused silica tube in a dry, nitrogen-filled glovebox. The tube was removed, evacuated to $\sim10^{-4}$ mbar then flame-sealed. It was then placed into a furnace where it heated to 850 °C, soaked for 24 h, then cooled to room temperature in 24 h. The product was irregular-shaped shiny black crystals of $Cs_4(Sn_3Se_8)[Sn(P_2Se_6)]_2$ (90%) and a small amount of $SnSe_2$ (10%).[49] EDS gave an average composition of multiple crystals of $Cs_4Sn_{4.9}P_{4.3}Se_{19.9}$. This material is air and water stable.

PHYSICAL MEASUREMENTS

High-Resolution In Situ PXRD with Synchrotron Radiation. In situ synchrotron PXRD were taken at beamline 17-BM-B in the Advanced Photon Source at Argonne National Laboratory running at 18 keV (λ = 0.72768 Å) with a PerkinElmer a-Si C-window detector at a distance of 500 mm. A dark frame was taken before each PXRD frame, and 35 1 s exposures were averaged together for each PXRD pattern. The capillary furnace setup translated horizontally across the entire capillary twice with respect to the synchrotron beam for every averaged PXRD pattern to obtain data of the entire capillary. An electrical resistance furnace detailed by Chupas et al. was used to heat the capillaries.[50] The samples were heated to 200 °C at a rate of 10 °C/min then further heated to 650 °C at 2 °C/min. With no soaking time at 650 °C, the capillaries cooled to 200 °C at a rate of 2 °C/min, then cooled further to room temperature at a rate of 10 °C/min. LaB_6 was used as the standard to refine the sample-to-detector distance and imaging plate tilt relative to the beam. The raw images were processed in GSAS II.[51] Peak matching of the data was conducted by

DOI: 10.1021/jacs.7b05423
J. Am. Chem. Soc. 2017, 139, 10814−10821

comparing calculated PXRD patterns obtained from the ICSD database to the experimental data.

Ex Situ PXRD. PXRD patterns were obtained from a Rigaku Miniflex600 diffractometer with Cu Kα radiation operating at 40 kV and 15 mA with a high-speed silicon strip detector. A zero-background Si sample holder with 0.2 mm indent was used. The experimental PXRD patterns were compared to simulated ones from CIFs using the FINDIT software for the ICSD.

Single Crystal XRD. Single crystals were fixed to glass fibers using super glue then analyzed in a STOE IPDS II single crystal diffractometer with Mo Kα radiation (λ = 0.71073 Å) operating at 50 kV and 40 mA. The STOE programs X-Area, X-RED, and X-SHAPE were used to conduct the data collection, integration, and numerical absorption, respectively. The atomic sites without disorder from the analogous $Rb_4Sn_5P_4Se_{20}$[52] were used to solve the crystal structure of $Cs_4(Sn_3Se_8)[Sn(P_2Se_6)]_2$ and SHELXT[53] was used to solve the crystal structures of $Cs_4Sn(P_2Se_6)_2$ and α-$Cs_2SnP_2Se_6$. The structures were all refined in the SHELXTL program package.[54] The twinning in α-$Cs_2SnP_2Se_6$ was subsequently refined using Jana2006.[55] Details on refining disorder and twinning are in the Supporting Information (SI). The CIFs were finalized using EnCIFer.[56]

Scanning Electron Microscopy (SEM). Semiquantitative microprobe analyses and EDS were performed on a Hitachi S-3400 scanning electron microscope equipped with a PGT energy-dispersive X-ray analyzer. For EDS, parameters of 25 kV accelerating voltage, 60 mA probe current, and 60 s acquisition time were used.

Solid-State UV/Vis/Near-IR Spectroscopy. Powdered samples were placed on a bed of $BaSO_4$, which was set to 100% reflectance. Diffuse reflection measurements from 200−2000 nm were taken using a Shimadzu UV-3600 PC double-beam, double-monochromator spectrophotometer. The Kubelka−Munk equation: $\alpha/S = (1 - R)^2/2R$, where R is reflectance, α is the absorption coefficient, and S is the scattering coefficient, was employed to convert the reflectance data into absorption.[46] The band gap was estimated by linearly fitting the absorption.

Differential Thermal Analysis (DTA). Granules of the sample (~80 mg) were flame-sealed in an ampule evacuated to ~10^{-4} mbar. An ampule of the standard, α-Al_2O_3, with a similar mass was also prepared. A Shimadzu DTA-50 thermal analyzer carried out the DTA experiments with parameters of ±5 °C/min rate and a maximum temperature of 650 °C. The temperature at the center of the peaks and valleys are reported as the crystallization and melting temperatures, respectively.

Transport Measurements. Transport measurements were conducted on $Cs_4(Sn_3Se_8)[Sn(P_2Se_6)]_2$ single crystals. Resistivity and Hall effect were measured on a Quantum Design PPMS-9T. Contacts were made with gold wires attached to the sample surface using carbon paste, and sample dimensions were obtained from SEM images.

RESULTS AND DISCUSSION

In Situ Synchrotron PXRD. We chose to explore the Cs/Sn/P/Se system because we have studied it previously and found the quaternaries $Cs_2SnP_2Se_6$[57] and $Cs_6Sn_2P_2Se_{14}$.[58] Being a known system to us presented the possibility to compare the effectiveness of the in situ approach we describe here to the conventional "blind" approach. We were also interested in answering the question of how these phases form and whether any intermediate phases existed, that had not been observed previously. $Cs_2SnP_2Se_6$ was picked as the starting point, and we decided to explore how the phase composition changes by varying the amount of tin in the Cs/P/Se flux. Figure 1a depicts the three reactions set up for in situ synchrotron PXRD. The three reactions are labeled as **Sn1**, **Sn2**, and **Sn3**, according to the equivalence of tin in the reaction.

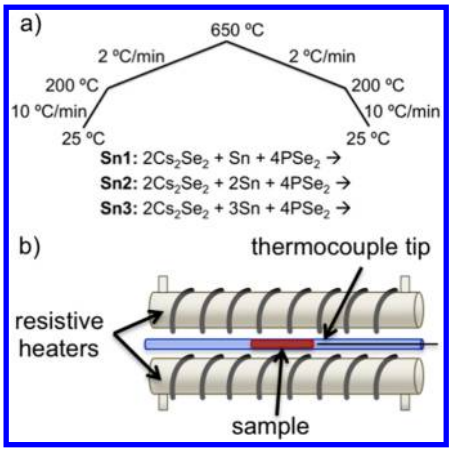

Figure 1. Experimental setup for in situ synchrotron PXRD: (a) Reaction procedure with the three reactions labeled as **Sn1**, **Sn2**, and **Sn3**, according to the equivalence of tin in the reaction. (b) Model of capillary furnace used.

A schematic of the glass capillary furnace used for the in situ synchrotron PXRD is shown in Figure 1b. PXRD patterns were continuously generated as the sample heated to 650 °C then cooled to room temperature. Each in situ experiment lasted ~8 h, and produced 486 PXRD patterns (Figure 2). All three

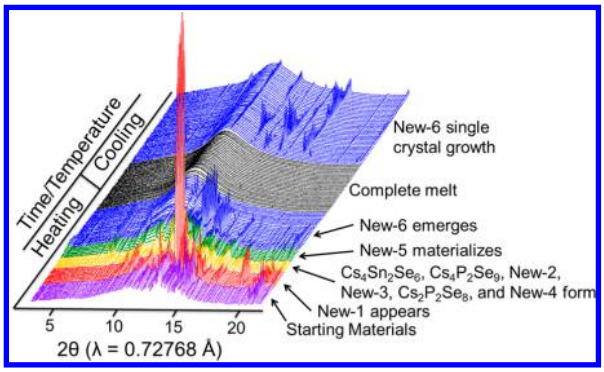

Figure 2. Select in situ synchrotron PXRD patterns every 10 °C exhibiting the entire reaction progression of **Sn1** to show a sample of the raw data collected. Color scheme: starting materials (purple); formation of **New-1** (red); formation of $Cs_4Sn_2Se_6$, $Cs_4P_2Se_9$, **New-2**, **New-3**, $Cs_2P_2Se_8$, and **New-4** (yellow); formation of **New-5** (green); formation of **New-6** (blue); and full melt (black).

experiments produced data that showed a complex phase space on heating, a full melt before 650 °C, and fewer phases on cooling. The number of phases present in the **Sn2** and **Sn3** experiments becomes so high around ~250 °C on heating that the peaks are no longer sharp and separated, and the identity of crystalline phases present can no longer be determined in confidence. However, **Sn2** and **Sn3** showed similar characteristics to **Sn1** overall, and some qualitative comparisons can still be made.

DOI: 10.1021/jacs.7b05423
J. Am. Chem. Soc. 2017, 139, 10814−10821

For the remainder of this paper we focus on the **Sn1** experiment because we were able to extensively analyze this in situ synchrotron PXRD data. The PXRD patterns of **Sn1** were compared to simulated patterns of the starting materials and all known combinations of Cs, Sn, P, and/or Se from the elements to quaternaries. Seven known crystalline phases were identified in this process: Sn,[40] Cs_2Se_3,[41] Cs_4Se_{16},[42] Cs_2Se_5,[43] $Cs_2Sn_2Se_6$,[44] $Cs_4P_2Se_9$,[45] and $Cs_2P_2Se_8$.[36] There were numerous unaccounted diffraction peaks remaining, and these were designated as 6 unique unknown phases based on the temperature of appearance and disappearance of each group of peaks. The amount of each phase present was estimated by comparing peak intensity between all PXRD frames as done previously.[10] The relationship between temperature and phases of the **Sn1** reaction are visualized in Figure 3 and summarized in Table 1. Below we describe what happens during the **Sn1** reaction.

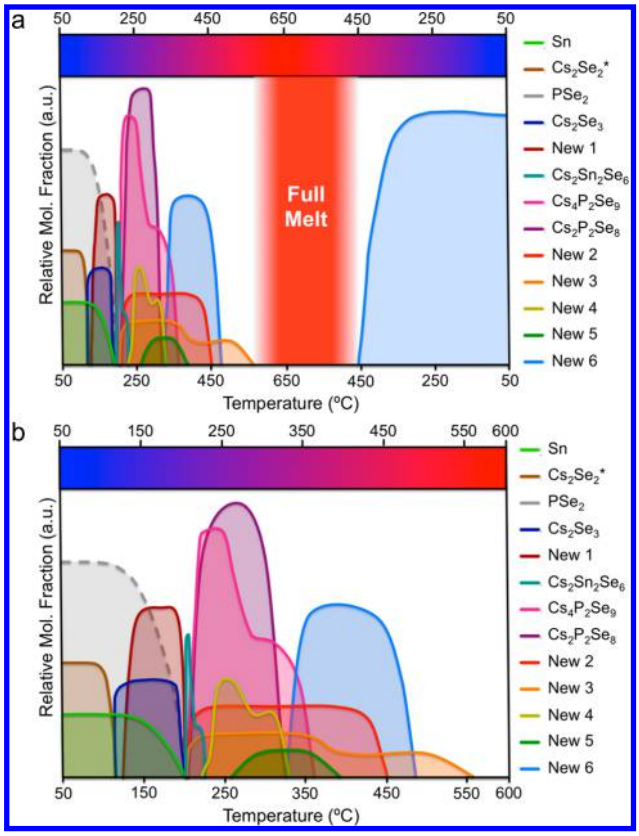

Figure 3. Reaction map of **Sn1**: (a) Full cycle; (b) On heating only. * = Nominal composition (the mixed crystalline phases that make up "Cs_2Se_2" are Cs_2Se_3, Cs_4Se_{16}, and Cs_2Se_5). Dashed lines represent noncrystalline phase present.

At the onset, all starting materials (Sn, "Cs_2Se_2", and PSe_2) are present. Sn is crystalline and easily identified in the in situ synchrotron PXRD.[40] "Cs_2Se_2" exists nominally; the synthesis procedure used to form Cs_2Se_2 yielded a mixture of cesium polyselenides with 3 crystalline stoichiometries (Cs_2Se_3,[41] Cs_4Se_{16},[42] and Cs_2Se_5[43]) that average together to nominal "Cs_2Se_2" when including mole percent. The final starting material, PSe_2, is amorphous, so its presence is unseen by PXRD. We presume that PSe_2 is present in the system until phosphorus-containing phases crystallize.

Table 1. Phases Observed from the In Situ Synchrotron PXRD of Sn1 Reaction

phase	start (°C)	end (°C)	heating or cooling
Sn[40]	RT	201	Heating
"Cs_2Se_2"[a]	RT	114	Heating
Glassy PSe_2[b]	RT	204	Heating
Cs_2Se_3[41]	114	201	Heating
New-1	125	204	Heating
$Cs_2Sn_2Se_6$[44]	204	224	Heating
$Cs_4P_2Se_9$[45]	206	363	Heating
New-2	206	450	Heating
New-3	206	560	Heating
$Cs_2P_2Se_8$[36]	211	322	Heating
New-4 α-$Cs_2SnP_2Se_6$	220	327	Heating
New-5 $Cs_4(Sn_3Se_8)[Sn(P_2Se_6)]_2$	261	389	Heating
New-6 $Cs_4Sn(P_2Se_6)_2$	323	483	Heating
New-6 $Cs_4Sn(P_2Se_6)_2$	444	RT	Cooling

[a]Nominally Cs_2Se_2; mixture of crystalline Cs_2Se_3,[41] Cs_2Se_5,[43] and Cs_4Se_{16}.[42] [b]Amorphous so not observed in PXRD, but it is a known starting material; end temperature presumed when crystalline P-containing phases appear.

On heating, nominal "Cs_2Se_2" anneals to preferentially give Cs_2Se_3[41] as the only cesium polyselenide present after 114 °C. Soon after at 125 °C, the first unknown phase, **New-1**, appears. This phase is short-lived, disappearing by 204 °C. The intensity of the Sn peaks remain strong around the temperature range of **New-1**, hence we do not expect **New-1** to contain Sn. Experiments to identify **New-1** ex situ indicated that it is very air sensitive.

Around 200 °C on heating, many changes occur: Sn,[40] Cs_2Se_3,[41] **New-1**, and PSe_2 react and ternaries begin to form. First is the transient $Cs_2Sn_2Se_6$[44] from 204 to 224 °C. $Cs_4P_2Se_9$[45] and two unknowns (**New-2** and **New-3**) appear at 206 °C. Both unknowns are present in the system for a range of over 150 °C. $Cs_2P_2Se_8$[36] emerges at 211 °C and is the most prominent phase until it dissipates at 322 °C. Three additional unknowns are seen on heating: **New-4** from 220 to 327 °C, **New-5** from 261 to 389 °C, and **New-6** from 323 to 483 °C. The final phase to melt is **New-3** at 560 °C. We will show below that **New-4**, **-5**, and **-6** are all quaternaries, and the known phases present in this temperature region are ternaries. From 560 °C up to 650 °C on heating, the entire sample is a full melt and all crystalline phases disappear. On cooling from 650 °C, the reaction mixture remains a melt until 444 °C, when **New-6** crystallizes. This is the only phase formed on cooling, and it remains until the end of the experiment at room temperature.

Once the relationship between temperature and phases has been established, the unknown phases can be identified. There are three main routes to identifying unknowns from in situ PXRD. First, the in situ PXRD can be used as a full guide to synthesize single crystals ex situ for characterization. Second, the structure can be deduced by chemical analogy to known compounds by comparing calculated PXRD patterns to the experimental in situ PXRD patterns. Third, computational software (e.g., FOX[59]) can be employed to solve structures from the in situ PXRD.

Additionally, examining how the intensity of a phase is affected by the presence of unknown phases gives additional information to help identify the unknowns. For example,

DOI: 10.1021/jacs.7b05423
J. Am. Chem. Soc. 2017, 139, 10814−10821

$Cs_4P_2Se_9$[45] and **New-4** both decrease in intensity when **New-5** forms on heating. It is therefore likely that **New-5**, $Cs_4P_2Se_9$,[45] and **New-4** all have similar structural building blocks, which can help us identify **New-4** and **New-5**. The anionic units (i.e., potential building blocks) of the known compounds seen in the in situ synchrotron PXRD of **Sn1** are depicted in Figure 4.

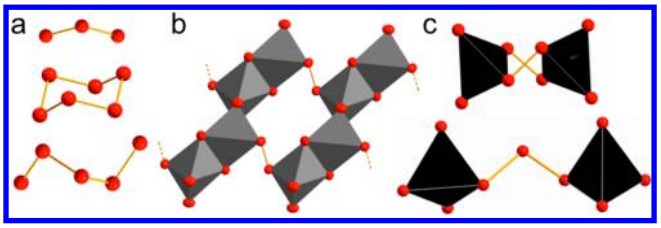

Figure 4. Structure of anionic units in known crystalline phases detected in **Sn1** in situ synchrotron PXRD experiment: (a) Polyselenide units in cesium polyselenides. (b) Part of $^2/_\infty[Sn_2Se_6]^{4-}$ layer with octahedrally coordinated Sn in $Cs_2Sn_2Se_6$.[44] (c) Molecular ions $[P_2Se_8]^{2-}$ and $[P_2Se_9]^{4-}$ with tetrahedrally coordinated P from $Cs_2P_2Se_8$[36] and $Cs_4P_2Se_9$,[45] respectively. Color scheme: selenium (red), tin (gray), phosphorus (black).

Identifying New-6 as $Cs_4Sn(P_2Se_6)_2$. The unknown, **New-6**, was identified using method 1 (i.e., synthesize ex situ). The major product of the **Sn1** reaction was **New-6** so this stoichiometric ratio was used along with a similar albeit longer heating profile. The product was hexagonal plate crystals of $Cs_4Sn(P_2Se_6)_2$. This material crystallizes in the trigonal space group $R\bar{3}$ with crystal parameters of a = 7.808(1) Å, c = 37.905(8) Å, V = 2001.4(6) Å^3, and Z = 3 (Table 2). It is comprised of molecular ions of $[Sn(P_2Se_6)_2]^{4-}$ charge balanced by Cs^+ cations (Figure 5). Sn has an oxidation state of +4 and

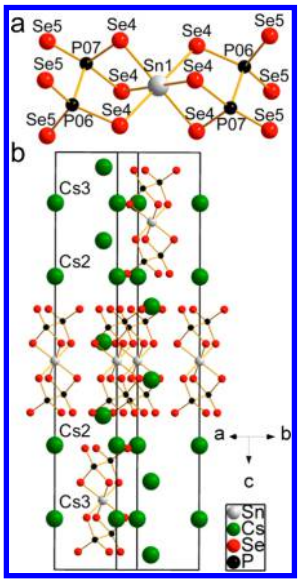

Figure 5. (a) Molecular ion of $[Sn(P_2Se_6)_2]^{4-}$. (b) Unit cell of $Cs_4Sn(P_2Se_6)_2$ viewed down the [540] direction. Disorder in the structure can be seen in Figure S10.

coordinates octahedrally to six total selenium atoms, three from each $[P_2Se_6]^{4-}$ ligand. The $[Sn(P_2Se_6)_2]^{4-}$ molecular ions sit in the middle of a $\bar{3}$ improper rotation; however, the molecules themselves do not possess this symmetry (D_{3d}). Therefore, the

Table 2. Crystal Refinements of $Cs_4Sn(P_2Se_6)_2$, α-$Cs_2SnP_2Se_6$, β-$Cs_2SnP_2Se_6$ (for Comparison to the α-Phase),[66] and $Cs_4(Sn_3Se_8)[Sn(P_2Se_6)]_2$[a]

structural formula	$Cs_4Sn(P_2Se_6)_2$ **New-6**	α-$Cs_2SnP_2Se_6$ **New-4**	β-$Cs_2SnP_2Se_6$ ref 66	$Cs_4(Sn_3Se_8)$ $[Sn(P_2Se_6)]_2$ **New-5**
Formula weight	1721.73	920.21	920.21	2828.17
Temperature (K)	293(2)	293(2)	100	293(2)
Wavelength (Å)	0.71073	0.71073	0.71073	0.71073
Crystal system	Trigonal	Monoclinic	Monoclinic	Trigonal
Space group	$R\bar{3}$	$P2_1/c$	$P2_1/c$	$P\bar{3}m1$
Unit cell dimensions	a = 7.808(1) Å	a = 10.230(1) Å	a = 10.116 Å	a = 7.695(1) Å
	b = 7.808(1) Å	b = 12.990(1) Å	b = 12.7867 Å	b = 7.695(1) Å
	c = 37.905(8) Å	c = 10.950(2) Å	c = 11.0828 Å	c = 18.797(4) Å
		β = 94.53(1)°	β = 94.463°	
V (Å^3)	2001.4(6)	1450.5(3)	1429.2(1)	964.0(3)
Z	3	4	4	1
Calculated ρ (g/cm^3)	4.285	4.213	4.277	4.872
μ (mm^{-1})	22.932	21.937	22.264	25.966
F(000)	2214	1576	1576	1210
Reflections collected	5141	11524	10599	9435
Independent reflections	942	2625	2955	1058
R_{int}	0.0769	0.1206	0.0670	0.0412
Completeness to θ = 25°	100%	100%	N/A	99.60%
Data/restraints/parameters	942/2/63	2625/0/101	N/A	1058/0/57
Goodness-of-fit	1.054	3.17	1.123	1.238
Final R indices [$>2\sigma(I)$]	R_{obs} = 0.0566	R_{obs} = 0.0691	R_{obs} = 0.0438	R_{obs} = 0.0397
	wR_{obs} = 0.1085	wR_{obs} = 0.1456	wR_{obs} = 0.0764	wR_{obs} = 0.0837
R indices [all data]	R_{all} = 0.0930	R_{all} = 0.0973	R_{obs} = 0.0650	R_{all} = 0.0473
	wR_{all} = 0.1241	wR_{all} = 0.1488	wR_{obs} = 0.0812	wR_{all} = 0.0865
Extinction coefficient	N/A	N/A	N/A	0.00111(16)
Largest diff. peak and hole (e·Å^{-3})	1.505 and −1.172	1.395 and −2.682	1.161 and −1.153	1.942 and −1.592

[a] $R = \Sigma||F_o| - |F_c||/\Sigma|F_o|$, $wR = \{\Sigma[w(|F_o|^2 - |F_c|^2)^2]/\Sigma[w(|F_o|^4)]\}^{1/2}$ and calc $w = 1/[\sigma^2(F_o^2) + (0.0234P)^2 + 0.0000P]$ where $P = (F_o^2 + 2F_c^2)/3$.

DOI: 10.1021/jacs.7b05423
J. Am. Chem. Soc. 2017, 139, 10814−10821

$[P_2Se_6]^{4-}$ units disorder into three positions to accommodate the D_{3d} symmetry (Figure S10). Additional details of the disorder are described in the SI. The structure of the molecular ion $[Sn(P_2Se_6)_2]^{4-}$ is analogous to $[M(P_2Se_6)_2]^{5-}$ (M = As, Bi, In) in $Cs_5As(P_2Se_6)_2$,[60] $Cs_5Bi(P_2Se_6)_2$,[61] and $Cs_5In(P_2Se_6)_2$,[62] which crystallize in the space groups $P4_2/m$, $Pmc2_1$, and $P4_2/m$, respectively.

$Cs_4Sn(P_2Se_6)_2$ can be synthesized as a pure phase by direct combination, and it is stable in air and water. It does not form a glass by water quenching the melt. Differential thermal analysis reveals congruent melting at 542 °C and recrystallization on cooling at 526 °C (Figure S11). This material has a band gap of 1.7 eV (Figure S12).

Identifying New-4 as α-$Cs_2SnP_2Se_6$. The **New-4** phase was identified using a combination of methods 1 and 2 (i.e., synthesize ex situ and chemical analogy, respectively). **New-4** has a similar PXRD pattern to the known one-dimensional $Cs_2SnP_2Se_6$[57] (Figure S13), hence their structures are possibly similar. **New-4** is also seen in the **Sn2** and **Sn3** in situ synchrotron PXRD, and with higher intensity in both as compared to **Sn1**. This gave evidence that **New-4** is a Sn-rich phase. On the basis of this information, we targeted synthesizing **New-4** ex situ with Sn ratios greater than that used in the **Sn1** in situ synchrotron PXRD experiment. The best sample with matching PXRD to **New-4** was formed using a Cs:Sn:P:Se stoichiometry of 2:1:2:6. EDS analysis confirmed the composition of the **New-4** orange rod crystals to be $Cs_2SnP_2Se_6$. The structure was determined at 293 K while the previously determined literature structure was solved at 100 K, thus we call these phases α- and β-$Cs_2SnP_2Se_6$, respectively. Both α- and β-$Cs_2SnP_2Se_6$ crystallize in the monoclinic space group $P2_1/c$ and have similar unit cell parameters (Table 2). The key structural difference between α- and β-$Cs_2SnP_2Se_6$ is that there is disorder in the $[P_2Se_6]^{4-}$ units in the β-phase, but there is no disorder in the α-phase. This alters the PXRD pattern slightly between the two similar phases (Figure S13). The structures of both phases are one-dimensional chains of $^1/_\infty[SnP_2Se_6]^{2-}$, which are composed of alternating Sn^{2+} and the ethane-like $[P_2Se_6]^{4-}$ units (Figure 6). The chains are charge-balanced by Cs^+ cations. Each Sn^{2+} ion has distorted seesaw geometry (Table S7) and coordinates to two $[P_2Se_6]^{4-}$ units, with two regular Sn−Se bonds and one nonbonding Sn−Se interaction per $[P_2Se_6]^{4-}$ unit. The lone pair on the Sn^{2+} center is therefore stereochemically expressed and alternates pointing up or down on in the chain. There are numerous examples of selenophosphate structures comprised of one-dimensional chains of $^1/_\infty[MP_2Se_6]^{2-}$ (M = Cd, Fe, Hg, Mn, Pd, Zn),[47,63−65] but α- and β-$Cs_2SnP_2Se_6$ are the first examples with seesaw metal coordination. Further in situ XRD studies of these two phases would reveal if there is a relationship between them, i.e., if one phase transitions into the other.

Identifying New-5 as $Cs_4(Sn_3Se_8)[Sn(P_2Se_6)]_2$. The structure of **New-5** was first hypothesized by method 2 (i.e., chemical analogy). The (001) peak of **New-5** has high intensity and an uncommonly low 2θ value ($2\theta_{(001)}$ = 2.24° with λ = 0.72768 Å and below we determine c = 18.797(4) Å). This easily identifiable peak along with the other peaks assigned to **New-5** were recognized as analogous to $Rb_4(Sn_3Se_8)[Sn(P_2Se_6)]_2$.[52] We deduced **New-5** to be $Cs_4(Sn_3Se_8)[Sn(P_2Se_6)]_2$ and synthesized it ex situ by following a modified literature procedure for $Rb_4(Sn_3Se_8)[Sn(P_2Se_6)]_2$.

$Cs_4(Sn_3Se_8)[Sn(P_2Se_6)]_2$ crystallizes in the trigonal space group $P\bar{3}m1$ with a = 7.695(1) Å, c = 18.797(4) Å, V = 964.0(3) Å^3, and Z = 1 (Table 2). The structure is analogous to $Rb_4(Sn_3Se_8)[Sn(P_2Se_6)]_2$[52] and is comprised of two-dimensional $^2/_\infty[Sn_3Se_8]^{4-}$ infinite slabs derived from the structure of $SnSe_2$ missing 1/4 of the Sn atoms;[49] these layers are capped by coordinating to one $[Sn(P_2Se_6)]$ fragment per side (i.e., two total) of each unit of the $^2/_\infty[Sn_3Se_8]^{4-}$ layer (Figure 7). The Sn^{4+} in $[Sn(P_2Se_6)]$ has octahedral coordination with three Se from the $^2/_\infty[Sn_3Se_8]^{4-}$ layer and three Se from $[P_2Se_6]^{4-}$. The resulting −4 charge is balanced by the four Cs^+ cations. Similar to $Cs_4Sn(P_2Se_6)_2$, the $[P_2Se_6]^{4-}$ units distort into three positions because they sit on a symmetry element they do

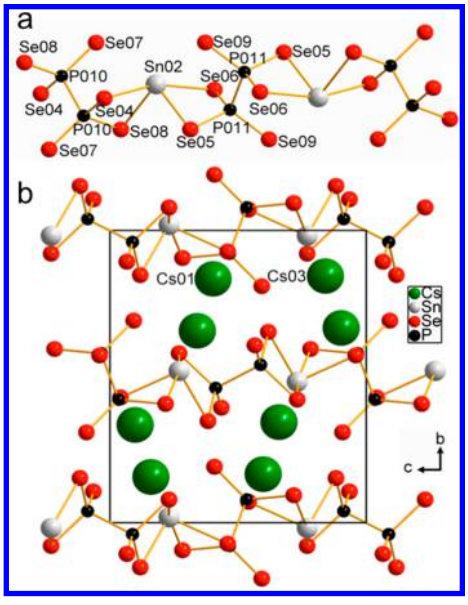

Figure 6. (a) Chain of $^1/_\infty[SnP_2Se_6]^{2-}$. (b) Unit cell of α-$Cs_2SnP_2Se_6$ viewed along the a-axis.

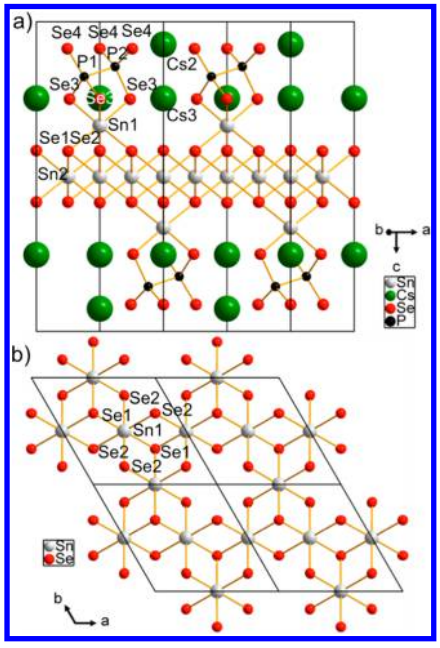

Figure 7. (a) Two unit cells of $Cs_4(Sn_3Se_8)[Sn(P_2Se_6)]_2$ viewed in the [010] direction. (b) $^2/_\infty[Sn_3Se_8]^{4-}$ layer viewed down the c-axis. Disordered P, Se, and Cs atoms removed for clarity. Disordered unit cell can be seen in Figure S14.

DOI: 10.1021/jacs.7b05423
J. Am. Chem. Soc. 2017, 139, 10814−10821

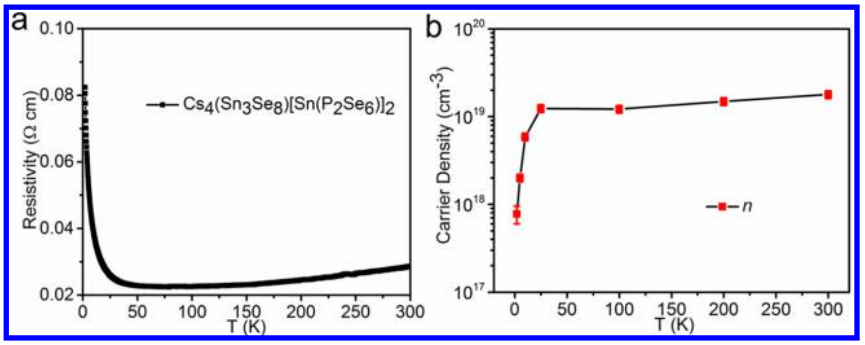

Figure 8. (a) Temperature-dependent resistivity. (b) Carrier density of $Cs_4(Sn_3Se_8)[Sn(P_2Se_6)]_2$.

not possess, namely C_{3v} (Figure S14). The Cs ions are disordered in the interlayer space. This material is air and water stable.

The targeted ex situ synthesis of $Cs_4(Sn_3Se_8)[Sn(P_2Se_6)]_2$ gave $SnSe_2$ as a minor second phase, but we were able to pick out single crystals large enough for electronic property measurements. Temperature-dependent resistivity and carrier density for $Cs_4(Sn_3Se_8)[Sn(P_2Se_6)]_2$ are shown in Figure 8. The resistivity decreases from 300 to 50 K and then increases with lower temperature. Compared to the resistivity of 0.0287 Ω·cm at 300 K, the one at 2 K (0.0824 Ω·cm) is comparable. The compound behaves as a heavily doped semiconductor. Hall resistivity has linear field dependent behavior and shows the material is n-type (Figure S15). As listed in Table S8, the calculated carrier concentration (n) at 300 K is $\sim 1.79 \times 10^{19}$ 1/cm^3. At 2 K, however, n decreased to be $\sim 7.78 \times 10^{17}$ 1/cm^3. This may be due to slight bandgap widening and subsequent carrier relaxation to the donor levels. The obtained mobilities ($\mu = 1/nq\cdot\sigma$) at 300 and 5 K are 12.2 cm^2/V·s and 97.5 cm^2/V·s, respectively. Clearly this fascinating set of compounds merit future details studies to full elucidate their properties.

CONCLUSION

In this work, we presented a powerful tool to discover new materials. The in situ synchrotron PXRD technique we employed yields a fingerprint of each crystalline phase present, including metastable intermediates, over a wide range of temperatures. Even previously investigated systems using the conventional "blind" approaches can yield new materials that have been missed. With just one stoichiometry in the Cs/Sn/P/Se system, stunningly we uncovered six new phases; three have been isolated and characterized, and three need further work to identify their structures and exact compositions. Because the in situ synchrotron PXRD monitoring of the reaction provides information on all occurring crystalline phases at once, it gives us total phase awareness under the specific reaction conditions. In this sense, it gives us a "panoramic" view of the reaction and provides the necessary evidence for where and when the compounds form and thus enabling the design of the synthesis. By conducting "panoramic synthesis", we are opening our eyes where we had been previously "blind" to what occurs during the "reaction arrow" of solid state synthesis. Our in situ synchrotron PXRD data described above provides clues to identifying the remaining unknowns for future studies. Panoramic synthesis is a powerful approach to accelerating materials discovery and can expand to a wide variety of new systems. We believe there is a multitude of new structures that panoramic synthesis can reveal where other synthetic techniques fall short. By developing this approach and combining with other in situ local structural techniques and molecular dynamics simulations, we can move toward better structure predictability and expedited discovery of inorganic materials.

ASSOCIATED CONTENT

Supporting Information

The Supporting Information is available free of charge on the ACS Publications website at DOI: 10.1021/jacs.7b05423.

Details of disorder and twinning, atomic coordinates, displacement parameters, in situ synchrotron PXRD patterns, figures of disorder in crystal structures, absorption spectra, DTA, and transport measurements (PDF)

X-ray crystallographic data of $Cs_4Sn(P_2Se_6)_2$, α-$Cs_2SnP_2Se_6$, and $Cs_4(Sn_3Se_8)[Sn(P_2Se_6)]_2$ (CIF)

AUTHOR INFORMATION

Corresponding Author

*m-kanatzidis@northwestern.edu

ORCID

Constantinos C. Stoumpos: 0000-0001-8396-9578

Mercouri G. Kanatzidis: 0000-0003-2037-4168

Notes

The authors declare no competing financial interest.

ACKNOWLEDGMENTS

We gratefully acknowledge support from the National Science Foundation Grant DMR-1708254 and a Graduate Research Fellowship for A. S. H. under Grant No DGE-1324585. This work made use of the EPIC facility of the NU*ANCE* Center at Northwestern University, funded by the Soft and Hybrid Nanotechnology Experimental (SHyNE) Resource (NSF NNCI-1542205); the MRSEC program (NSF DMR-1121262) at the Materials Research Center; the International Institute for Nanotechnology (IIN); the Keck Foundation; and the State of Illinois, through the IIN. A. S. H. acknowledges Prof. Daniel Shoemaker for his guidance on analyzing the in situ PXRD and Ms. Charlotte Stern for her crystallography mentorship.

REFERENCES

(1) Demazeau, G. *J. Mater. Sci.* **2008**, *43*, 2104−2114.
(2) Feng, S.; Xu, R. *Acc. Chem. Res.* **2001**, *34*, 239−247.
(3) Gopalakrishnan, J. *Chem. Mater.* **1995**, *7*, 1265−1275.
(4) Gopalakrishnan, J.; Bhuvanesh, N. S. P.; Rangan, K. K. *Curr. Opin. Solid State Mater. Sci.* **1996**, *1*, 285−294.

DOI: 10.1021/jacs.7b05423
J. Am. Chem. Soc. 2017, 139, 10814−10821

(5) Kanatzidis, M. G. *Curr. Opin. Solid State Mater. Sci.* **1997**, *2*, 139−149.
(6) Kanatzidis, M. G.; Sutorik, A. C. *Prog. Inorg. Chem.* **1995**, *43*, 151−265.
(7) Liu, X.; Fechler, N.; Antonietti, M. *Chem. Soc. Rev.* **2013**, *42*, 8237−8265.
(8) Walton, R. I. *Chem. Soc. Rev.* **2002**, *31*, 230−238.
(9) Yu, J.; Xu, R. *Acc. Chem. Res.* **2010**, *43*, 1195−1204.
(10) Shoemaker, D. P.; Hu, Y.-J.; Chung, D. Y.; Halder, G. J.; Chupas, P. J.; Soderholm, L.; Mitchell, J. F.; Kanatzidis, M. G. *Proc. Natl. Acad. Sci. U. S. A.* **2014**, *111*, 10922−10927.
(11) Francis, R. J.; O'Brien, S.; Fogg, A. M.; Halasyamani, P. S.; O'Hare, D.; Loiseau, T.; Ferey, G. *J. Am. Chem. Soc.* **1999**, *121*, 1002−1015.
(12) Christensen, A. N.; Convert, P.; Lehmann, M. S. *Acta Chem. Scand.* **1980**, *34*, 771−776.
(13) Walton, R. I.; O'Hare, D. *Chem. Commun.* **2000**, 2283−2291.
(14) Pienack, N.; Bensch, W. *Angew. Chem., Int. Ed.* **2011**, *50*, 2014−2034.
(15) Engelke, L.; Schaefer, M.; Schur, M.; Bensch, W. *Chem. Mater.* **2001**, *13*, 1383−1390.
(16) Engelke, L.; Schaefer, M.; Porsch, F.; Bensch, W. *Eur. J. Inorg. Chem.* **2003**, *2003*, 506−513.
(17) Kiebach, R.; Pienack, N.; Ordolff, M.-E.; Studt, F.; Bensch, W. *Chem. Mater.* **2006**, *18*, 1196−1205.
(18) Pienack, N.; Näther, C.; Bensch, W. *Eur. J. Inorg. Chem.* **2009**, *2009*, 937−946.
(19) Turrillas, X.; Barnes, P.; Gascoigne, D.; Turner, J. Z.; Jones, S. L.; Norman, C. J.; Pygall, C. F.; Dent, A. J. *Radiat. Phys. Chem.* **1995**, *45*, 491−508.
(20) Cheetham, A. K.; Mellot, C. F. *Chem. Mater.* **1997**, *9*, 2269−2279.
(21) Geselbracht, M. J.; Noailles, L. D.; Ngo, L. T.; Pikul, J. H.; Walton, R. I.; Cowell, E. S.; Millange, F.; O'Hare, D. *Chem. Mater.* **2004**, *16*, 1153−1159.
(22) Biswas, K.; Zhang, Q.; Chung, I.; Song, J.-H.; Androulakis, J.; Freeman, A. J.; Kanatzidis, M. G. *J. Am. Chem. Soc.* **2010**, *132*, 14760−14762.
(23) Xiong, W.-W.; Zhang, G.; Zhang, Q. *Inorg. Chem. Front.* **2014**, *1*, 292−301.
(24) Xiong, W.-W.; Zhang, Q. *Angew. Chem., Int. Ed.* **2015**, *54*, 11616−11623.
(25) Haynes, A. S.; Saouma, F. O.; Otieno, C. O.; Clark, D. J.; Shoemaker, D. P.; Jang, J. I.; Kanatzidis, M. G. *Chem. Mater.* **2015**, *27*, 1837−1846.
(26) Kanatzidis, M. G. In *Encyclopedia of Inorganic and Bioinorganic Chemistry*; Wiley, 2006.
(27) Morris, C. D.; Chung, I.; Park, S.; Harrison, C. M.; Clark, D. J.; Jang, J. I.; Kanatzidis, M. G. *J. Am. Chem. Soc.* **2012**, *134*, 20733−20744.
(28) Chung, I.; Malliakas, C. D.; Jang, J. I.; Canlas, C. G.; Weliky, D. P.; Kanatzidis, M. G. *J. Am. Chem. Soc.* **2007**, *129*, 14996−15006.
(29) Chung, I.; Do, J.; Canlas, C. G.; Weliky, D. P.; Kanatzidis, M. G. *Inorg. Chem.* **2004**, *43*, 2762−2764.
(30) Chung, I.; Jang, J. I.; Gave, M. A.; Weliky, D. P.; Kanatzidis, M. G. *Chem. Commun.* **2007**, 4998−5000.
(31) Breshears, J. D.; Kanatzidis, M. G. *J. Am. Chem. Soc.* **2000**, *122*, 7839−7840.
(32) Vysochanskii, Y. *Ferroelectrics* **1998**, *218*, 275−282.
(33) Banerjee, S.; Malliakas, C. D.; Jang, J. I.; Ketterson, J. B.; Kanatzidis, M. G. *J. Am. Chem. Soc.* **2008**, *130*, 12270−12272.
(34) Chung, I.; Song, J.-H.; Kim, M. G.; Malliakas, C. D.; Karst, A. L.; Freeman, A. J.; Weliky, D. P.; Kanatzidis, M. G. *J. Am. Chem. Soc.* **2009**, *131*, 16303−16312.
(35) Wang, P. L.; Liu, Z.; Chen, P.; Peters, J. A.; Tan, G.; Im, J.; Lin, W.; Freeman, A. J.; Wessels, B. W.; Kanatzidis, M. G. *Adv. Funct. Mater.* **2015**, *25*, 4874−4881.
(36) Haynes, A. S.; Banerjee, A.; Saouma, F. O.; Otieno, C. O.; Jang, J. I.; Kanatzidis, M. G. *Chem. Mater.* **2016**, *28*, 2374−2383.
(37) Jang, J. I.; Park, S.; Harrison, C. M.; Clark, D. J.; Morris, C. D.; Chung, I.; Kanatzidis, M. G. *Opt. Lett.* **2013**, *38*, 1316−1318.
(38) Chung, I.; Kanatzidis, M. G. *Chem. Mater.* **2014**, *26*, 849−869.
(39) Brant, J. A.; Clark, D. J.; Kim, Y. S.; Jang, J. I.; Zhang, J. H.; Aitken, J. A. *Chem. Mater.* **2014**, *26*, 3045−3048.
(40) Swanson, H. E.; Tatge, E.; Fuyat, R. K. *Standard X-ray Diffraction Powder Patterns*; U.S. Dept. of Commerce, National Bureau of Standards: Washington, D.C., 1953.
(41) Böttcher, P. *Z. Anorg. Allg. Chem.* **1980**, *461*, 13−21.
(42) Sheldrick, W. S.; Braunbeck, H. G. *Z. Naturforsch., B: J. Chem. Sci.* **1989**, *44*, 1397−1401.
(43) Kretschmann, U.; Bottcher, P. *Z. Naturforsch., B: J. Chem. Sci.* **1985**, *40*, 895−899.
(44) Klepp, K. O.; Fabian, F. *Z. Kristallogr. - New Cryst. Struct.* **1998**, *213*, 17.
(45) Chondroudis, K.; Kanatzidis, M. G. *Inorg. Chem.* **1995**, *34*, 5401−5402.
(46) McCarthy, T. J.; Ngeyi, S. P.; Liao, J. H.; Degroot, D. C.; Hogan, T.; Kannewurf, C. R.; Kanatzidis, M. G. *Chem. Mater.* **1993**, *5*, 331−340.
(47) McCarthy, T. J.; Kanatzidis, M. G. *Inorg. Chem.* **1995**, *34*, 1257−1267.
(48) Okazaki, A.; Ueda, I. *J. Phys. Soc. Jpn.* **1956**, *11*, 470−470.
(49) Minagawa, T. *J. Phys. Soc. Jpn.* **1980**, *49*, 2317−2318.
(50) Chupas, P. J.; Chapman, K. W.; Kurtz, C.; Hanson, P. L.; Grey, C. P. *J. Appl. Crystallogr.* **2008**, *41*, 822−824.
(51) Toby, B. H.; Von Dreele, R. B. *J. Appl. Crystallogr.* **2013**, *46*, 544−549.
(52) Chung, I.; Biswas, K.; Song, J. H.; Androulakis, J.; Chondroudis, K.; Paraskevopoulos, K. M.; Freeman, A. J.; Kanatzidis, M. G. *Angew. Chem., Int. Ed.* **2011**, *50*, 8834−8838.
(53) Sheldrick, G. M. *Acta Crystallogr., Sect. A: Found. Adv.* **2015**, *71*, 3−8.
(54) Sheldrick, G. M. *Acta Crystallogr., Sect. A: Found. Crystallogr.* **2008**, *A64*, 112−122.
(55) Petříček, V.; Dušek, M.; Palatinus, L. *Z. Kristallogr. - Cryst. Mater.* **2014**, *229*, 345−352.
(56) Allen, F. H.; Johnson, O.; Shields, G. P.; Smith, B. R.; Towler, M. *J. Appl. Crystallogr.* **2004**, *37*, 335−338.
(57) Chung, I.; Kanatzidis, M. G. *Inorg. Chem.* **2010**, *50*, 412−414.
(58) Chondroudis, K.; Kanatizidis, M. G. *Chem. Commun.* **1996**, 1371−1372.
(59) Favre-Nicolin, V.; Černý, R. *J. Appl. Crystallogr.* **2002**, *35*, 734−743.
(60) Morris, C. D.; Kanatzidis, M. G. *Inorg. Chem.* **2010**, *49*, 9049−9054.
(61) Chung, I.; Song, J.-H.; Jang, J. I.; Freeman, A. J.; Ketterson, J. B.; Kanatzidis, M. G. *J. Am. Chem. Soc.* **2009**, *131*, 2647−2656.
(62) Chondroudis, K.; Chakrabarty, D.; Axtell, E. A.; Kanatzidis, M. G. *Z. Anorg. Allg. Chem.* **1998**, *624*, 975−979.
(63) Chondroudis, K.; Kanatzidis, M. G. *J. Solid State Chem.* **1998**, *138*, 321−328.
(64) Chondroudis, K.; Kanatzidis, M. G.; Sayettat, J.; Jobic, S.; Brec, R. *Inorg. Chem.* **1997**, *36*, 5859−5868.
(65) Haynes, A. S.; Lee, K.; Kanatzidis, M. G. *Z. Anorg. Allg. Chem.* **2016**, *642*, 1120−1125.
(66) Chung, I.; Kanatzidis, M. G. *Inorg. Chem.* **2011**, *50*, 412−414.

DOI: 10.1021/jacs.7b05423
J. Am. Chem. Soc. 2017, 139, 10814−10821